THE JOURNAL OF PHYSICAL CHEMISTRY C

ARTICLE

pubs.acs.org/JPCC

Orientation-Dependent Room-Temperature Ferromagnetism of FeSi Nanowires and Applications in Nonvolatile Memory Devices

Shih-Wei Hung,[†] Terry Tai-Jui Wang,[‡] Li-Wei Chu,[†] and Lih-Juann Chen*[,†]

[†]Department of Materials Science and Engineering, National Tsing Hua University, Hsinchu 30013, Taiwan, Republic of China

[‡]Department of Materials Science and Engineering, National Chiao Tung University, Hsinchu 30010, Taiwan, Republic of China

ABSTRACT: Self-catalyzed growth of FeSi nanowires has been achieved via a spontaneous chemical reaction method. The room-temperature ferromagnetism behavior compared to that of bulk FeSi at 4 K is attributed to the enhancement of magnetic coupling behavior correlated to different crystalline orientations. The resistivity of the single-stem FeSi nanowire was determined to be 2650 $\mu\Omega\cdot$cm. The fabricated memory devices based on FeSi nanowires showed significant $C-V$ hysteresis, exhibiting the memory effect. The strong memory effect can be accounted for by the presence of defects or dangling bonds on the surface of the FeSi nanowires embedded in the SiO_2 layer, which enhances the trapping density for nonvolatile memory applications.

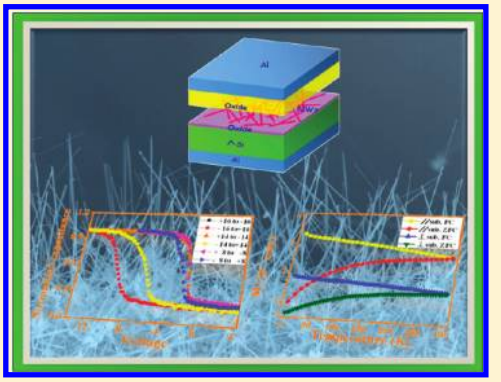

INTRODUCTION

One-dimensional nanowires have been the focus of scientific interest due to their potential applications in electronic and optoelectronic nanodevices.[1−7] These nanostructures exhibit fascinating physical and chemical properties distinct from those of bulk or thin film materials.[8−10] Among them, for the synthesis of 1-D nanowires, metal-catalyzed chemical vapor deposition (CVD) has proven to be one of the most successful growth methods.[11−14] However, metal contaminations are often detrimental to their applications.[15] Growth by a spontaneous chemical vapor transport method without catalyst is favored if the method proves to be a viable alternative.

Transition-metal silicides are significant as an integral part of complementary metal−oxide−semiconductor (CMOS) devices. Recently, magnetic nanowires exhibiting ferromagnetism have received considerable attention as attractive candidates for magnetic storage and spintronic nanodevice applications.[16,17] In addition, ferromagnetic nanowires can be applied as a racetrack memory in which the magnetic domain is acting as data bits controlled by applying spin polarized current.[18]

On the other hand, memory cell structures using nanostructures as the charge storage media have received much attention for future high-speed and low power consumption memory devices.[19,20] Nanocrystals embedded in SiO_2 layers have been widely studied, and strong memory effects in MOS devices were obtained.[21] Furthermore, using nanowires to replace nanocrystals in a nonvolatile memory (NVM) device has been reported.[22] The memory devices using nanowires have displayed several advantages such as weaker Coulomb blockade effect, less quantum confinement effect, and the compatibility with the conventional silicon technology, compared to the zero-dimensional nanocrystals.[23]

FeSi has been of keen experimental and theoretical interest for decades due to its narrow band gap behavior, and it was the only known transition metal Kondo insulators.[24] For high-quality single crystalline FeSi, a very weak ferromagnetic behavior has been detected and it was attributed to the uncompensated magnetic Fe ions in samples.[25] For the electrical resistivity, FeSi exhibits specific semiconductor-to-metal transition behavior at particular places in the Brillouin zone.[26] In this paper, we report direct growth and structural characterization of the single crystalline FeSi nanowires via a spontaneous chemical vapor transport method. The orientation-dependent room temperature ferromagnetism behavior compared with bulk FeSi at 4 K is reported. In addition, strong memory effects using FeSi nanowires as the trapping centers were found. The favorable properties shall be conducive to applications in spintronic nanodevices, magnetic recording media, and nonvolatile memory devices.

EXPERIMENTAL SECTION

Iron silicide nanowires were synthesized in a horizontal hot wall two-zone furnace by a chemical vapor transport method. During the growth of iron silicide nanowires, a constant gas flow of 120 SCCM (SCCM denotes cubic centimeter per minute at STP) carrier gas of Ar was introduced. The Si substrates were cleaned with 3% buffered HF prior to being placed in the furnace. $FeCl_3\cdot 4H_2O$ powders used as the precursor and Si(001) as the substrates were placed in the upstream and downstream zones, respectively. The upstream and downstream zones were heated from room temperature to 650 and 850 °C, respectively. After

Received: February 12, 2011
Revised: May 29, 2011
Published: July 19, 2011

dx.doi.org/10.1021/jp201395r | *J. Phys. Chem. C* 2011, 115, 15592–15597

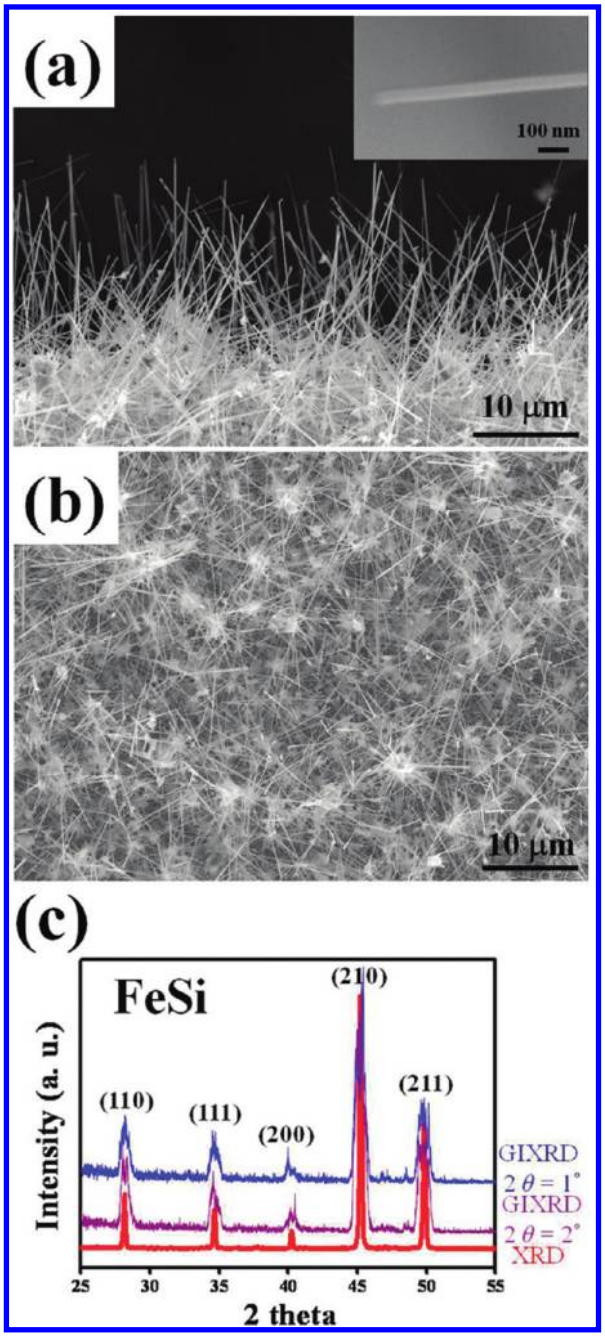

Figure 1. (a) Cross-section SEM image of the free-standing FeSi nanowires grown at the downstream zone. Inset: higher magnification image. (b) Top view SEM image showing the FeSi nanowires. (c) XRD and GIXRD spectra, all the peaks can be ascribed to the FeSi phase.

the set temperature was reached, the samples were annealed for 2 h and then cooled down to room temperature slowly. The morphology of the iron silicide nanowires was examined with a field-emission scanning electron microscope (FESEM) (JEOL JSM-6500F). The crystal structures of the as-synthesized nanowires were determined by X-ray diffraction (XRD) and grazing incident X-ray diffraction (GIXRD). The microstructures and chemical compositions of the iron silicide nanowires were analyzed using a 200 kV transmission electron microscope (TEM) (JEOL JEM-2010) equipped with an energy dispersive spectrometer (EDS). For electrical property measurements, a focused ion beam (FIB) system was used to deposit a platinum layer as contacts at the edges of FeSi nanowires dispersed on the SiO_2/Si substrates. The magnetic properties were characterized by a superconducting quantum interference device magnetometer (SQUID). For capacitance−voltage ($C-V$) measurements, p-type silicon wafers were cleaned with standard RCA process, followed by a dry oxidation to form a 5 nm thick tunneling oxide. Subsequently, FeSi nanowires were dispersed onto the tunneling oxide. The FeSi nanowires were capped by a control oxide layer of 100 nm. Finally, Al gate electrode was patterned and sintered. The measurements were performed using a precision LCR meter HP 4284A to study the electron charging effects of the FeSi nanowires.

RESULTS AND DISCUSSION

Figure 1a is the representative cross-section SEM image showing free-standing FeSi nanowires with diameters from 20 to 40 nm and lengths from 20 to 30 μm. The aspect ratio of the FeSi nanowire is more than 500. Inset shows the high-magnification SEM image of a 40 nm nanowire. Figure 1b is the top view SEM image. The growth of high density nanowires over large area can be achieved in our growth system. GIXRD and XRD spectra are shown in Figure 1c. For the GIXRD ($2\theta = 1°$ and $2\theta = 2°$) spectra, surface signals were obtained and all diffraction peaks can be ascribed to the FeSi phase with a B-20 cubic structure. For the XRD spectrum obtained from the same sample, only FeSi phase was detected, which is consistent with the GIXRD results.

Figure 2a shows the low-magnification TEM image of an individual FeSi nanowire with a diameter of 27 nm. Figure 2b shows a SAED pattern, obtained from a representative nanowire that can be ascribed to the FeSi phase. It also demonstrates that the nanowire growth is along the [10−1] direction. The EDS spectrum, shown in Figure 2c, indicates that the nanowire is composed of Fe and Si with an atomic ratio close to 1:1. The corresponding high-resolution TEM image, as shown in Figure 2d, reveals the single-crystalline structure of the nanowire free from linear or planar defects. The two d-spacings of 0.317 and 0.317 nm correspond to interspacings of FeSi (1−10) and (10−1) planes, respectively.

The reactions of the evaporated $FeCl_3$ precursor vapor with the silicon substrates at the hot zone of the furnace to form the FeSi nanowires may follow two reaction pathways

$$4FeCl_{3(g)} + 7Si_{(s)} \rightarrow 4FeSi_{(s)} + 3SiCl_{4(g)}$$

$$2FeCl_{3(g)} + 2SiCl_{4(g)} \rightarrow 2FeSi_{(s)} + 7Cl_{2(g)}$$

No catalyst particles were found at the tips of the nanowires, suggesting that our nanowire growth was not via the typical vapor−liquid−solid growth mechanism.[27] The growth of the FeSi nanowires apparently followed the vapor−solid mechanism by a self-catalytic process.[28,29] At 850 °C, only high aspect ratio FeSi nanowires were obtained. On the other hand, sheet structure was found to grow at lower temperatures.

The electrical properties of the single-stem FeSi nanowires were measured by the four-terminal $I-V$ method at room temperature. The current output as a function of applied voltage of a FeSi nanowire is shown in Figure 3. The fabricated measurement structure is depicted in the inset. The obtained resistivity of the 60 nm FeSi nanowire is 2650 $\mu\Omega\cdot$cm. Kim and Bird[30] reported the specific electrical characteristics as well as ferromagnetic properties of the $FeSi_2$ nanowires. The $FeSi_2$ nanowires

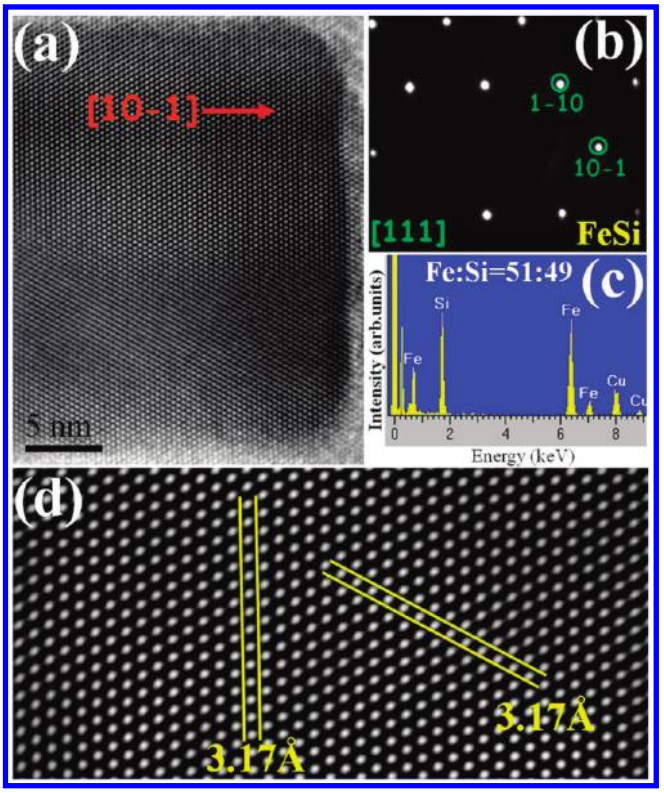

Figure 2. TEM analyses of the FeSi nanowires: (a) high-resolution image showing the growth direction is along [10−1]; (b) SAED pattern confirms the formation of single-crystalline FeSi with cubic structure; (c) EDS analysis shows chemical composition of Fe:Si is close to 1:1; (d) atomic resolution image also confirms the nanowire is FeSi.

fabricated by the reactive epitaxy method showed the resistances near 100 kΩ. On the other hand, the FeSi nanowires we report herein exhibit a resistance of 56.5 kΩ. In electrical transport measurements, both $FeSi_2$ and FeSi nanowires show the Ohmic contact characteristic between nanowires and the contact electrodes. Both β-$FeSi_2$ and FeSi are semiconductors, and the obtained resistances of 50−100 kΩ showed semiconducting characteristics. Kim and Bird attributed the high value of the $FeSi_2$ resistance to the combined influence of interfacial scattering and slight process-related damage. In the present work, the estimated resistivity of 2650 $\mu\Omega\cdot$cm obtained herein is 1 order higher than that reported in previous works (Schmitt et al.,[31] 210 $\mu\Omega\cdot$cm; Paschen et al.,[25] 165 $\mu\Omega\cdot$cm). The much higher resistivity value is attributed to the surface scattering effect and rough interface induced in the nanodevice fabrication processes (removal of surface silicon oxide or Pt deposition by FIB).[30] In general, the influence of contact resistance is significant for two-terminal single-stem nanowire measurements. Seo et al.[32] has reported the resistivities of Fe_5Si_3 nanowires by four terminal measurements, and two terminal measurements were estimated to be 487 and 881 $\mu\Omega\cdot$cm, respectively. This increase in resistivity was attributed to the contact resistance.

The detailed magnetic properties of the FeSi nanowires grown along the [10−1] direction were studied by SQUID. Temperature-dependent field cooling (FC) and zero-field cooling (ZFC) magnetization measurements at various applied field directions are shown in Figure 4a. The magnetic field of 200 Oe was applied parallel and perpendicular to the substrates, respectively. As shown in our data, $M-T$ curves of the as-synthesized FeSi

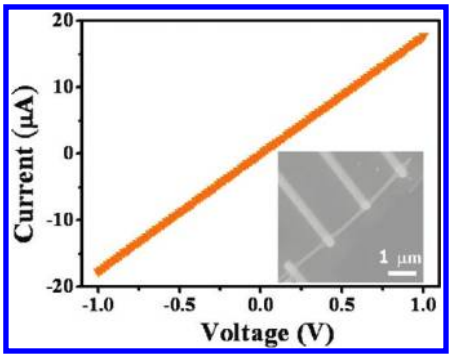

Figure 3. Electrical transport measurement of a single-stem FeSi nanowire at room temperature. Inset: SEM image of the FeSi nanowire with Pt electrodes.

nanowires show typical ferromagnetic behavior with a Curie temperature above room temperature. FC and ZFC curves of FeSi nanowires do not overlap at temperatures lower than room temperature, indicating the existence of large magnetic anisotropic energy in FeSi nanowires system.[33] A similar magnetic anisotropic energy effect also induces the enhancement in magnetization while the applied field was parallel to the substrates in contrast to that perpendicular to the substrates. In typical metals, the magnetic property of the magnetoresistance (MR) effect was attributed to the quantum-mechanical weak localization (WL) at low temperature.[34] However, for semiconducting silicon, the possibility of magnetism was accounted for by the ordering of the unpaired spins associated with naturally occurring dangling bonds (DBs).[35,36] These surface-induced DBs play an important role in magnetic characteristics in nanomaterials. In the present work, the magnetic properties of FeSi nanowires with very thin native oxide layers were investigated. The specific room-temperature ferromagnetic properties in FeSi nanowires can be accounted for by the interaction of charge carriers (electrons or holes) with localized dangling bond spins, which is significant when the system size is reduced to the nanoscale.[37]

In order to gain further insight into the magnetic properties of the FeSi nanowire assembly, the magnetization as a function of magnetic field was measured at various temperatures as shown in Figure 4b. The applied magnetic field was parallel to the substrates. The nonlinear hysteresis loop curve shows that the FeSi nanowires exhibit ferromagnetic behavior at room temperature. The coercive field (Hc) and residual magnetization (Mr) were found to increase with decreasing temperature due to the reduction of the thermal fluctuation. For bulk monosilicide FeSi, it was reported that a very weak ferromagnetism was observed at 4 K even for high-quality single crystals.[25,38] A distinctive hysteresis loop curve can be observed when measurement temperature was down to 2 K, as shown in Figure 4c. The hysteresis loop for the case of the applied magnetic field parallel to the substrates has a relatively hard magnetization axis and high residual magnetization. On the other hand, the hysteresis loop for the case of the applied magnetic field perpendicular to the substrate has an easy magnetization axis and low residual magnetization. As shown in our data, the high remanence in nanowires is attributed to the shape anisotropy effect, which forces the magnetic moments to mostly align along the axis of the nanowires.[39]

Recently, a large hysteretic MR feature of silicide nanostructures was reported when the system size is reduced to nanoscale.[37] Seo et al. reported that single crystalline CoSi

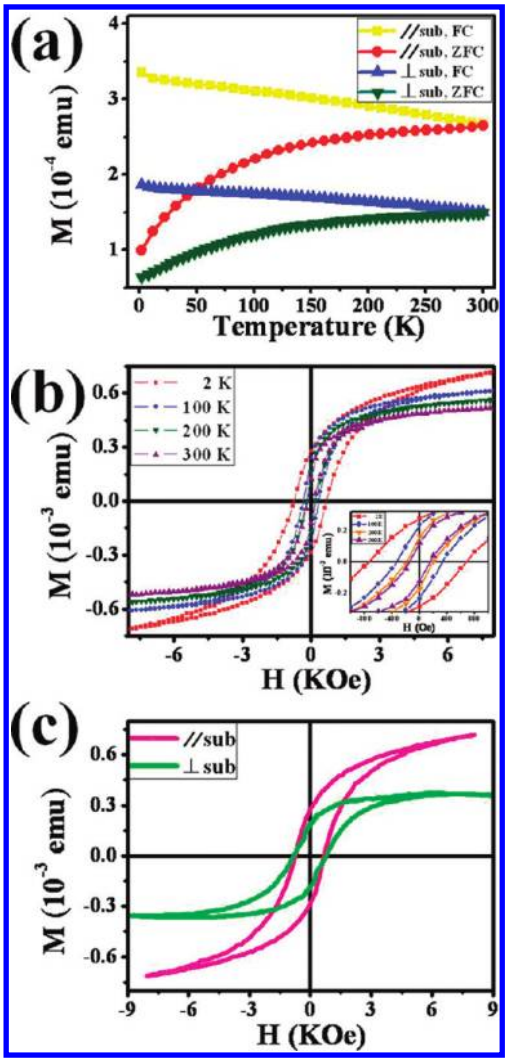

Figure 4. Magnetic properties of the as-grown FeSi nanowires. (a) $M-T$ curves of the as-synthesized FeSi nanowires, showing the typical ferromagnetic behavior with a Curie temperature above room temperature. Temperature-dependent FC and ZFC magnetization measurements illustrated at the magnetic fields applied both parallel and perpendicular to the substrates. (b) $M-H$ curves of the FeSi nanowires measured at various temperatures, indicating room temperature ferromagnetism behavior of the FeSi nanowires. The inset shows the loops on an enlarged scale. (c) Hysteresis loop curve of FeSi nanowires performed at 2 K. The magnetic field was applied both parallel and perpendicular to the substrates.

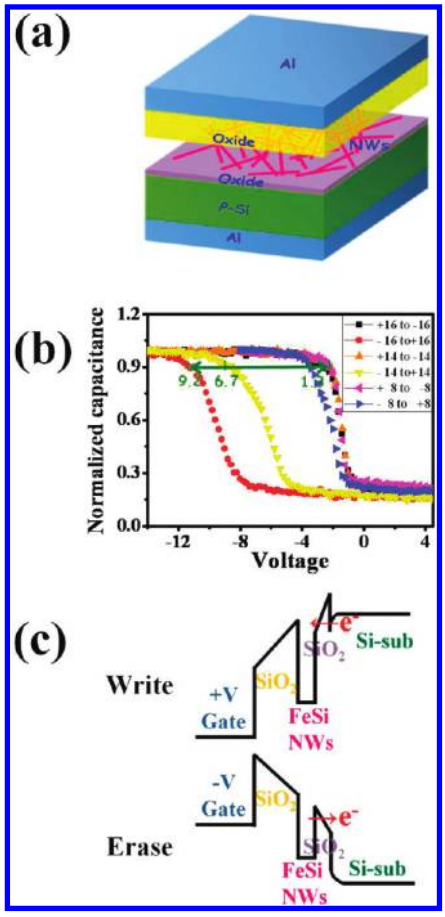

Figure 5. (a) The schematic plot of the stacking memory structure. (b) The $C-V$ hysteresis curves of FeSi nanowire memory devices, indicating the memory effect of FeSi nanowires embedded in SiO_2. (c) The band diagram of write and erase operations of the memory device.

nanowires exhibit ferromagnetism property, in contrast to the diamagnetic CoSi in bulk.[16] The room temperature ferromagnetism was attributed to the strain or structure defects in crystal or reduced coordination of the surface metal atoms in silicide nanowires. FeSi nanowires with B-20 cubic structure and grown along [111] were reported to exhibit very weak ferromagnetism at the temperature below 300 K.[40] It has been demonstrated that the ferromagnetism of the nanowires depended strongly on nanowires' crystalline orientations, which is attributed to the cooperative contributions of both magnetocrystalline anisotropy and shape anisotropy.[41] In our TEM images shown in Figure 2, the as-synthesized FeSi nanowires grown along [10−1] exhibit not only different crystalline orientation but also higher atomic packing density than nanowires grown along [111]. The existing magnetic domain and localized surface dangling bond spins may enhance the performance of the magnetic coupling behavior more significantly. The investigation by Liang et al.[42] focused on the epitaxial heterojunctions and magnetic properties of the Fe_3O_4 nanoparticles (NPs) capped on FeSi nanowires (NWs) with the growth axis of [110]. The epitaxial relationships of heterojunctions and specific ferromagnetism behaviors were also investigated. In their magnetic properties measurement, the MH curve of Fe_3O_4 NPs/FeSi NWs performed at 300 K shows a coercive field of 60 Oe, which also suggested ferromagnetism obtained from Fe_3O_4 NPs/FeSi NWs, at room temperature. On the other hand, the superparamagnetic properties of Fe_3O_4 NPs have been reported extensively,[43−45] which implied a negligible or near zero coercive field at room temperature. Room temperature ferromagnetism can therefore be attributed to FeSi nanowires.

The schematic stacking structure of the memory device using FeSi nanowires is shown in Figure 5a. The stacking structure of the "Al/SiO_2/FeSi nanowires/SiO_2/p−Si-sub/Al" memory device was tested under different sweeping ranges of gate voltage. The forward and reverse sweep $C-V$ characteristics for the memory effect measurements at room temperature are shown in Figure 5b. A clear hysteresis behavior is observed, showing the electron charging and discharging effects of FeSi nanowires embedded in the SiO_2 layer. The double $C-V$ sweeps were

dx.doi.org/10.1021/jp201395r |J. Phys. Chem. C 2011, 115, 15592–15597

performed from the inversion region to accumulation region and in reverse, which exhibit a strong electron charging effect. Dai et al.[22] reported memory effects of carbon nanotubes as charge storage nodes and a memory window of 400 mV swept from 3 to (−3) V was found. As shown in our data, voltage swept from 8 to (−8) and back to 8 V, and a higher memory window width of 1.3 V for FeSi nanowires embedded in SiO_2 layer is observed. As the swept gate voltage is increased to 14 and 16 V, more significant $C-V$ shifts of 6.7 and 9.2 V are found, respectively. The strong memory effect can be accounted for by the presence of the defects or dangling bonds on the surface of the FeSi nanowires embedded in the SiO_2 layer, which would enhance the trapping density in our memory device for NVM applications. Comparative studies suggested that there are additional advantages in using transition metal silicide nanostructures for NVM applications. The memory effect caused by traps at the nanocrystals/oxide interface and an enhancement in charge storage capacity and retention time were studied.[21,46−48] In addition, investigations on the memory effect of the defects and charge traps correlated to the oxidation surface of the 1-D nanostructure were also reported.[22,49] In the present case, the dangling bonds and defects existing in native oxide/iron silicide nanowire are likely acting as the charge storage traps which result in the hysteresis memory effect. For comparison, the control samples without FeSi nanowires embedded in silicon oxide were also investigated (not shown here). No memory effect was found under ±10 V gate voltage operation. The shift toward the negative bias (∼−2 V) is attributed to the positive fixed charges within silicon oxide to satisfy the electric neutrality. Figure 5c shows the band diagram of "write" and "erase" operations of a memory device. When the device is written, electrons directly tunnel from Si substrates through tunneling oxide and are trapped by FeSi nanowires. On the other hand, when the device memory is erased, the electrons may tunnel back to the deep accumulation layer of Si substrates. The control oxide is applied to preventing carriers injecting from the gate electrode to FeSi nanowires by Fowler−Nordheim tunneling.[21] By our method to fabricate the FeSi nanowires embedded in the SiO_2 layer for potential application as NVM devices, a threshold voltage of 1.3 V can be defined as "1" and "0" by a typical sensing amplifier.

SUMMARY AND CONCLUSIONS

In summary, self-catalytic growth of FeSi nanowires with high aspect ratio has been achieved via a spontaneous chemical reaction method. The resistivity of single-stem FeSi nanowire was determined to be 2650 $\mu\Omega\cdot$cm. The room temperature ferromagnetism behavior with respect to bulk FeSi at 4 K is attributed to the enhancement of magnetic coupling behavior correlated to different crystalline orientation. Fabricated memory devices swept from 8 to (−8) V exhibit a memory window of 1.3 V, indicating electron charging and discharging effects. A more significant $C-V$ shift was obtained while the swept gate voltage is increased. A strong memory effect can be accounted for by the defects or dangling bonds existing on the surface of the FeSi nanowires embedded in SiO_2 layer. On the basis of the room-temperature ferromagnetism as well as favorable memory effect of fabricated devices, FeSi nanowires are applicable in Si-based spintronic nanodevices and NVM applications.

AUTHOR INFORMATION

Corresponding Author

*E-mail: ljchen@mx.nthu.edu.tw.

ACKNOWLEDGMENT

The research was supported by the Republic of China National Science Council Grants NSC 98-2221-E-007-169-MY3.

REFERENCES

(1) Zhong, Z.; Wang, D.; Cui, Y.; Bockrath, M. W.; Lieber, C. M. *Science* **2003**, *302*, 1377.
(2) Chen, K. C.; Wu, W. W.; Liao, C. N.; Chen, L. J.; Tu, K. N. *Science* **2008**, *321*, 1066.
(3) Huang, Y.; Duan, X.; Cui, Y.; Lauhon, L.; Kim, K. −H.; Lieber, C. M. *Science* **2001**, *294*, 1313.
(4) Schmitt, A. L.; Higgins, J. M.; Jin, S. *Nano Lett.* **2008**, *8*, 810.
(5) Chen, L. J. *J. Mater. Chem.* **2007**, *17*, 4639.
(6) Chou, Y. C.; Wu, W. W.; Cheng, S. L.; Yoo, B. Y.; Myung, N.; Chen, L. J.; Tu, K. N. *Nano Lett.* **2008**, *8*, 2194.
(7) Chou, Y. C.; Wu, W. W.; Chen, L. J.; Tu, K. N. *Nano Lett.* **2009**, *9*, 2337.
(8) Lu, W.; Lieber, C. M. *Nat. Mater.* **2007**, *6*, 841.
(9) Hochbaum, A. I.; Chen, R.; Delgado, R. D.; Liang, W.; Garnett, E. C.; Najarian, M.; Majumdar, A.; Yang, P. *Nature* **2008**, *451*, 163.
(10) Hsin, C. L.; Mai, W.; Gu, Y.; Gao, Y.; Huang, C. T.; Liu, Y.; Chen, L. J.; Wang, Z. L. *Adv. Mater.* **2008**, *20*, 1.
(11) Wang, Y.; Lew, K. -K.; Ho, T. -T.; Pan, L.; Novak, S. W.; Dickey, E. C.; Redwing, J. M.; Mayer, T. S. *Nano Lett.* **2005**, *5*, 2139.
(12) Garnett, E. C.; Liang, W.; Yang, P. *Adv. Mater.* **2007**, *19*, 2946.
(13) Tian, B.; Zheng, X.; Kempa, T. J.; Fang, Y.; Yu, N.; Yu, G.; Huang, J.; Lieber, C. M. *Nature* **2007**, *449*, 885.
(14) Wu, Y.; Fan, R.; Yang, P. *Nano Lett.* **2002**, *2*, 83.
(15) Oh, S. H.; Benthem, K. v.; Molina, S. I.; Borisevich, A. Y.; Luo, W.; Werner, P.; Zakharov, N. D.; Kumar, D.; Pantelides, S. T.; Pennycook, S. J. *Nano Lett.* **2008**, *8*, 1016.
(16) Seo, K.; Varadwaj, K. S. K.; Mohanty, P.; Lee, S.; Jo, Y.; Jung, M. −H.; Kim, J.; Kim, B. *Nano Lett.* **2007**, *7*, 1240.
(17) Beach, G. S. D.; Nistor, C.; Knutson, C.; Tsoi, M.; Erskine, J. L. *Nat. Mater.* **2005**, *4*, 741.
(18) Parkin, S. S. P.; Hayashi, M.; Thomas, L. *Science* **2008**, *320*, 190.
(19) Tiwari, S.; Rana, F.; Hanafi, H.; Hartstein, A.; Crabbé, E. F.; Chan, K. *Appl. Phys. Lett.* **1996**, *68*, 1377.
(20) Liu, Z.; Lee, C.; Narayanan, V.; Pei, G.; Kan, E. C. *IEEE Trans. Electron Devices* **2002**, *49*, 1606.
(21) Yeh, P. H.; Yu, C. H.; Chen, L. J.; Wu, H. H.; Liu, P. T.; Chang, T. C. *Appl. Phys. Lett.* **2005**, *87*, 193504.
(22) Lu, X. B.; Dai, J. Y. *Appl. Phys. Lett.* **2006**, *88*, 113104.
(23) Tsui, B.-Y.; Wang, P.-Y.; Chen, T.-Y.; Cheng, J.-C. *Microelectron. Reliab.* **2010**, *50*, 603.
(24) Aeppli, G.; DiTusa, J. F. *Mater. Sci. Eng., B* **1999**, *63*, 119.
(25) Paschen, S.; Felder, E.; Chernikov, M. A.; Degiorgi, L.; Schwer, H.; Ott, H. R. *Phys. Rev. B* **1997**, *56*, 12916.
(26) Klein, M.; Menzel, D.; Doll, K.; Neef, M.; Zur, D.; Jursic, I.; Schoenes, J.; Reinert, F. *New J. Phys.* **2009**, *11*, 023026.
(27) Morales, A. M.; Lieber, C. M. *Science* **1998**, *279*, 208.
(28) Chang, C. M.; Chang, Y. C.; Chung, Y. A.; Lee, C. Y.; Chen, L. J. *J. Phys. Chem. C* **2009**, *113*, 17720.
(29) Guiton, B. S.; Gu, Q.; Prieto, A. L.; Gudiksen, M. S.; Park, H. *J. Am. Chem. Soc.* **2002**, *127*, 498.
(30) Kim, T.; Bird, J. P. *Appl. Phys. Lett.* **2010**, *97*, 263111.
(31) Schmitt, A. L.; Bierman, M. J.; Schmeisser, D.; Himpsel, F. J.; Jin, S. *Nano Lett.* **2006**, *6*, 1617.
(32) Seo, K.; Lee, S.; Jo, Y.; Jung, M.-H.; Kim, J.; Churchill, D. G.; Kim, B. *J. Phys. Chem. C* **2009**, *113*, 6902.
(33) Bagkar, N.; Seo, K.; Yoon, H.; In, J.; Jo, Y.; Kim, B. *Chem. Mater.* **2010**, *22*, 1831.
(34) Bergmann, G. *Phys. Rep.* **1984**, *107*, 1.
(35) Bird, C. F.; Bowler, D. R. *Surf. Sci.* **2003**, *531*, L351.
(36) Sheka, E. F.; Nikitina, E. A.; Zayets, V. A. *Surf. Sci.* **2003**, *532−535*, 754.

(37) Kim, T.; Naser, B.; Chamberlin, R. V.; Schilfgaarde, M. V.; Bennett, P. A.; Bird, J. P. *Phys. Rev. B* **2007**, *76*, 184404.
(38) Arushanov, E.; Respaud, M.; Broto, J. M.; Leotin, J.; Askenazy, S.; Kloc, Ch.; Bucher, E.; Lisunov, K. *Phys. Rev. B* **1997**, *55*, 8056.
(39) Chueh, Y. L.; Chou, L. J.; Song, J.; Wang, Z. L. *Nanotechnology* **2007**, *18*, 145604.
(40) Ouyang, L.; Thrall, E. S.; Deshmukh, M. M.; Park, H. *Adv. Mater.* **2006**, *18*, 1437.
(41) Huang, X.; Li, L.; Luo, X.; Zhu, X.; Li, G. *J. Phys. Chem. C* **2008**, *112*, 1468.
(42) Liang, S.; Fang, X.; Xia, T. −L.; Qing, Y.; Guo, Z. −H. *J. Phys. Chem. C* **2010**, *114*, 16187.
(43) Tian, Y.; Yu, B.; Li, X.; Li, K. *J. Mater. Chem.* **2011**, *21*, 2476.
(44) Zhang, Y.; Xu, S.; Luo, Y.; Pan, S.; Ding, H.; Li, G. *J. Mater. Chem.* **2011**, *21*, 3664.
(45) Gao, G.; Liu, X.; Shi, R.; Zhou, K.; Shi, Y.; Ma, R.; Takayama-Muromachi, E.; Qiu, G. *Cryst. Growth Des.* **2010**, *10*, 2888.
(46) Jang, Y. S.; Yoon, J. H. *IEEE Trans. Electron Devices* **2009**, *56*, 3236.
(47) Kim, J. H.; Yang, J. Y.; Lee, J. S.; Hong, J. P. *Appl. Phys. Lett.* **2008**, *92*, 013512.
(48) Wang, T. T. J.; Chu, C. L.; Hsieh, I. J.; Tseng, W. S. *Appl. Phys. Lett.* **2010**, *97*, 143507.
(49) Cui, J. B.; Sordan, R.; Burghard, M.; Kern, K. *Appl. Phys. Lett.* **2002**, *81*, 3260.